NRIAG JOURNAL OF ASTRONOMY AND GEOPHYSICS
2024, VOL. 13, NO. 1, 165–181
https://doi.org/10.1080/20909977.2024.2402157

Hydrogeophysical investigations for assessment of groundwater aquifer at Wadi El Assuity, Egypt

Sultan Awad Araffa[a], Hassan S. Sabet[b], Ahmed M. El Zahar[c], Mahmoud S. Sharkawy[d] and Noha M. Hassan[e]

[a]Geomagnetic and Geoelectric, National Research Institute of Astronomy and Geophysics (NRIAG), Cairo, Egypt; [b]Faculty of Science, Geology Department, Al-Azhar University, Cairo, Egypt; [c]Geology Department, Egyptian Countryside Development Company, Cairo, Egypt; [d]Department of Petroleum Geology, Faculty of Petroleum and Mining Sciences, Matrouh University, Matrouh, Egypt; [e]Faculty of Science, Menofia University, Menofia, Egypt

ABSTRACT

Wadi El Assuity is one of the longest wadis in the Eastern Desert of Egypt. The main target of the present study is delineating the groundwater aquifer and defining the suitable sites for drilling. The interpretation of magnetic data refers to the basement rocks in the research area located between 1800 and over 4500 m below the ground surface, the main trends of subsurface structures area N-S, NE-SW, and NW-SE. The geoelectric data interpretation indicates that the aquifer's depth ranges from 6 to 18.4 m, and thickness ranges from 150 to 250 m, with resistivity values of 4–30 Ohm.m.

ARTICLE HISTORY
Received 23 February 2024
Revised 23 July 2024
Accepted 3 September 2024

KEYWORDS
Resistivity; hydrogeology; groundwater; basement; structures

1. Introduction

The decrease in water resources is a big problem for Egypt, especially now. Most desert areas in Egypt are suffering from scarcity of surface water, especially Wadi El-Assiuty; it represents the main promising desert area for future development; for this reason, groundwater exploration is very important to locate the sites of groundwater aquifer of low depths and high thickness with good water quality. The entrance to Wadi El-Assuity, Egypt's most significant wadi, is located east of Assiut City (Figure 1). Wadi El-Assuity spans an area of roughly 127 m^2, 186 km long and 10 km wide. The area under study is represented topographically by low land and variation in elevation from 52 to 182 m, and it is surrounded by a carbonate plateau with an elevation of 455 m above sea level. Numerous geologists have conducted numerous research on the study region in the fields of geology, geophysics, and hydrogeology, including Mohamed et al. (2021); El Miligy (2003); Abdo et al. (2021); Farrag et al. (2018) Mohamed (2013) and Youssef and Mansour (1977). They concluded that they estimate the depth of the upper surface of the aquifer in the study area. The present study aims to delineate the depth of the upper and lower surface of the aquifer, the thickness of the aquifer, water quality through hydrochemical analysis, structural elements that control the distribution of water flow in the aquifer, and the depth of basement rocks in the area under study. The geophysical tools can be used for subsurface structures, engineering geology, groundwater exploration, and ore mineral exploration (Sultan and Santos 2008; Mohamed et al. 2012; Deep et al. 2021; Elbarbary et al. 2021; Nazih et al. 2022; Araffa et al. 2022; Azmy et al. 2023). The eastern watershed area's recharge to the Quaternary aquifer is $5.6 \times 106\ m^3$ per year, and the flow to the outlet of Wadi El-Assuity is $6 \times 106\ m^3$ per year, or about 7% of the total annual precipitation calculated a $25.7 \times 106\ m^3$/year upward leakage from the aquifers beneath the Nubian Sandstone. As a result, the Quaternary aquifer system receives a total of around $33.7 \times 106\ m^3$/year, which is only enough to irrigate 2185 ha based on the water need of 2509 m^3/year (Yan et al. 2004; Yousef 2008).

2. Geological setting

Wadi El-Assuity is mainly covered by many recent sediments such as Wadi filing, sub-recent alluvium cover, Neonile and Prenile sediments Paleonile-Protonile sediments overlaying Lower Eocene limestone bedrock, many fault elements of NE-SW, NW-SE and N-S trends dissect the area under study (Figure 1). The sharp escarps of limestone bound Wadi El-Assiuty at the northern, southern, and eastern parts, but the western part was bounded by the Nile floodplain. According to Mansour and Philobbos (1983); and Said (1990), the subsurface sequences are represented by Holocene sediments (Figure 1), including two formations; the first is Recent wadi deposits comprising sand & gravel and fanglomerate. The second formation, known as the Arkin Formation, is composed of a 20-metre-thick silty clay layer that serves as the conventional agricultural clay

CONTACT Sultan Awad Araffa sultan_awad@yahoo.com National Research Institute of Astronomy and Geophysics, Al Marsed Street, Helwan, Cairo 11722, Egypt

layer in the Nile Valley in the Assuit region. The Abbasia, Dandara, and Dandara formations, where the Abbasia Formation is composed of gravels and sand, comprise Middle and Upper Pleistocene deposits. Sand intercalated with silt makes up the Dandara Formation. Sand and gravel with clay intercalation make up the Qena Formation. The Middle and Upper Pleistocene sediments are regarded as the primary Quaternary aquifer in the Assuit region because they unconformably overlie the formerly silt clay layer. Issawia, Armant, and Idfu formations are made of lower Pleistocene rock (Figure 1). The sand and clay strata of the Issawia Formation are topped by breccia. Conglomerate layers, clay, and sand form the Armant Formation. In Wadi El-Assuity, both the Armant and Issawia formations are seen (Figure 1). Gravel is found in the clayey matrix of the Idfu Formation. Deposits from the Pliocene period are made up primarily of clay facies. Carbonate rocks with chert bands make up the rocks of the Lower and Middle Eocene periods. The plateau that surrounded the Nile Valley on both sides is built up with these rocks (Figure 1(b,c)). The area under investigation is part of the Nile Valley. It is located on Egypt's stable shelf, where the primary fault systems are NW-SE, NE-SW, and N-S, according to the structural framework of the area (Youssef 1968; El Shemi et al. 1999). The area under study can be hydrogeological divided into Quaternary (Wadi deposits aquifer, Prenile aquifer, Protonile aquifer), and Eocene Aquifer systems, as indicated in the Table 1, according to Yousef (2008). The hydrogeological environment of the examined area may be affected by NW active fault networks, which are transporting more freshwater from the deep aquifer (Nubian sandstone) to the shallower aquifer. Freshwater samples with low salinities were primarily found near NW fault plains. The water level ranges from 50 to 60 m, as shown in Table 2.

3. Data and methodology

In the study region, aeromagnetic and geoelectric represented by Vertical Electrical Sounding (VES) techniques are used to locate structural features and define the depth of magnetic sources (crystalline rocks). To determine the depth of the aquifer, 29 VES points with AB/2 ranging from 1.5 to 500 m were conducted to evaluate these targets. The data was collected in 2017.

3.1. Aeromagnetic data acquisition

The Western Digital Company (1983), Ramadan and Sultan (2004), and others have all supplied aeromagnetic data as part of their surveys of Egypt. The

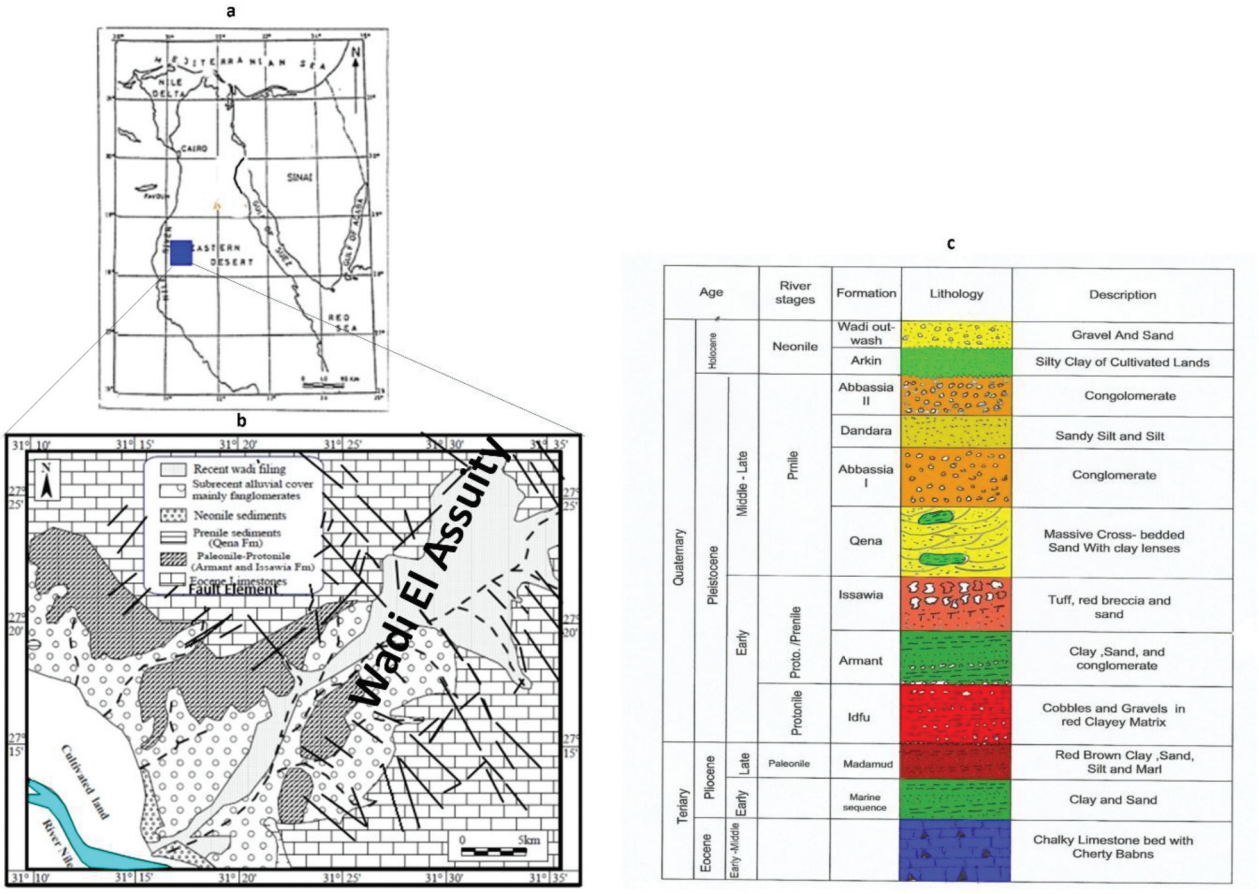

Figure 1. Location map of the study area, b: Geologic map with main fault systems of the study area (after said 1981 and Yousef 2008), c: composite stratigraphic cross section of the study area (after said 1981 and 1990).

Table 1. Hydrogeological data of the study area after Yousef (2008).

No.	Aquifer	Water bearing	Location according NW faults	Well name	Elevation (m)	Total depth (m)	Depth to water (m)	Water level (m)
1	**Quaternary**	Wadi deposits	High block of first fault	Pizometer 2 for 15 (F3)	109	200	87	22
2			High block of second fault	Hassan Salem (H. D.)	70	41	18.5	51.5
3		Prenile	Down block of first fault	Pizometer 1 for 15 (F3)	108	200	93	15
4		Mixed from wadi deposits and prenile	High block of first fault	Saad Mousa (No. 15)	109	174	58.5	50.5
5			Down block of first fault	Gamal Abdel Motal (8)	105	200	–	–
6				Esam El Sherif (33)	120	184	46	74
7			High block of second fault	Governorate (2)	87	200	–	–
8				Governorate (6)	86	200	–	–
9				Ibrahim Abu El Ayun (1)	181	200	–	
10			Down block of second fault	Hamed El Sebaey	83	130	28	55
11				Assuit Pump Station	81	200	72.4	8.6
12				Dr. Bosina El Said	79	126	34	45
13		Mixing between wadi deposits, prenile and protonile	High block of first fault	Ahmed Sarwat	118	206	61	57
14				Production (14)	108	202	85	23
15				Production (15)	103	192	–	–
16				Ibrahim Abu El Ayun (2)	106	192	53	53
17				Ashraf Abdel Rahman	108	180	72.3	35.7
18				Production (5)	89	180	70	19
19				Gamal Hassan	89	140	55	34
20			Down block of first fault	Wadea Maksemos (18)	110	175	60.2	49.8
21				Gamal Abdel Motal (9)	107	190	45	62
22				Magdy Asham (10)	93	173	48	45
23				Sameh Kohel	100	190	–	–
24			High block of second fault	Wageh El Gohary (35)	109	179	57	52
25				Kamel Abdel Naser (32)	120	150	50	70
26				Osman Ahmed	91	195	–	–
27				Production (20)	91	180	–	–
28				Roshdy	92	200	–	–
29				Governorate (13)	88	195	–	–
30			Down Block of second fault	Governorate (10)	85	180	–	–
31				Governorate (12)	81	174	52	29
32				Assuit 2000	88	190	–	–
33				Governorate (16)	80	240	28	52
34				Esam El Sherif (34)	115	280	43	72
35				Hag Abdel Wahab	90	186.5	30	60
36	**L.Eocene**	L. Eocene	High block of first fault	Pizometer 3 for 15 (F3)	109	600	61	48

Table 2. Chemical analysis of groundwater samples.

Location																			
Long	Lat	Sample No.	Total depth	Water level	Total hardness	T.D.S mg/l	SAR	Sodium content Na%	EC µ mohs/cm	MAR	PH	K^+ mg/l	Na^+ mg/l	Mg^{++} mg/l	Ca^{++} mg/l	CL^- mg/l	$SO4^-$ mg/l	$HCO3^-$ mg/l	$CO3^-$ mg/l
31.40570207	27.29640133	1	200	50	1128	2888	5.18	40.7	3374	33.6	7.9	85.5	400	92	300	476	830	695	4.337
31.414333	27.274278	2	200	50	210	1855	18.6	86.3	2674	71.5	8.05	3.6	620	36.48	24	840	160	152	16.76
31.38459458	27.27758038	3	174	50	2230.9	6474	8.66	44.8	6684	36.8	8.2	144.1	988	220	624	1176	1954	1360	16.67
31.393056	27.263333	4	200	50	183.72	6076	27.1	81.1	7569	63.3	7.95	7	1950	150.8	144	3200	520	112	1.311
31.37075134	27.26645354	5	200	50	816.26	2260	5.01	43.7	2756	31.8	8.1	83	329	63	223	370	653	525	12.32
31.386111	27.254167	6	200	52	242.77	1752	12.01	76	2566	36.4	8.12	4.4	520	31.1	89.6	800	165	148	0.8122
31.364833	27.25075	7	202	55	124.67	2013	13.01	76.3	2958	45.1	7.5	3	600	43.77	88	960	240	76	0.538
31.38363514	27.22455028	8	140	55	880.87	2144	5.08	44.2	2964	30.6	8.1	86	350	67	250	476	630	537	15.97
31.365694	27.223389	9	186	60	199	1080	9.54	77	1597	50	7.6	4	310	24.3	40	440	70.3	188	1.489
31.37568556	27.20217821	10	173	60	419	1326	4.59	49	1736	28.5	8.5	59	216	29	120	231	370	299	0.6035
31.34046071	27.23934663	11	195	50	585.6	1878	5.14	46.8	2405	30.6	8	78	297	47	176	347	571	354	3.375
31.32867341	27.26988628	12	280	50	348.53	1174	4.82	5.3	1554	28.4	8.6	43	207	24	100	224	280	293	1.682
31.33292232	27.22893001	13	186.5	60	190.28	819	3.33	45	1205	43.9	8.1	51	126	29	61	175	259	116	0.8016
31.33511531	27.19554946	14	195	60	519.99	1893	3.8	37.3	2434	35.8	7.9	98	239	65	192	294	686	317	0.8917

Aeromagnetic survey was conducted along a series of parallel flight lines with tie lines spaced out at 10-km intervals and orientated in a northeast-southwest direction. Using twin-engine Cessna-404 Titan-type aircraft, the total magnetic intensity was measured at 92-metre intervals with a nominal sensor altitude of 120-metre terrain clearance using a Varian V-85 proton precession magnetometer (sensitivity = 0.1 nano Tesla "nT") installed in a tail stinger arrangement as its principal sensor element (Aero-Service 1985). These data are represented by a total magnetic intensity map after being corrected by Western Digital Company for diurnal fluctuation and International Geomagnetic Reference Field (IGRF) (Figure 2a). The numbers on this map represent magnetic anomalies between 41,610 and 41,920 nT. The measured magnetic data is represented as the total magnetic intensity data (TMI), as shown in Figure 2a, after applying different corrections such as diurnal variation and IGRF. To overcome the distortion in anomalous characteristics, TMI is reduced to the (RTP) as in Figure 2(b). The reduction to the pole is applied using magnetic parameters like inclination (39°), declination (2°), and magnetic field strength (41715 nT) by Oasis Montaj (2015). The RTP map

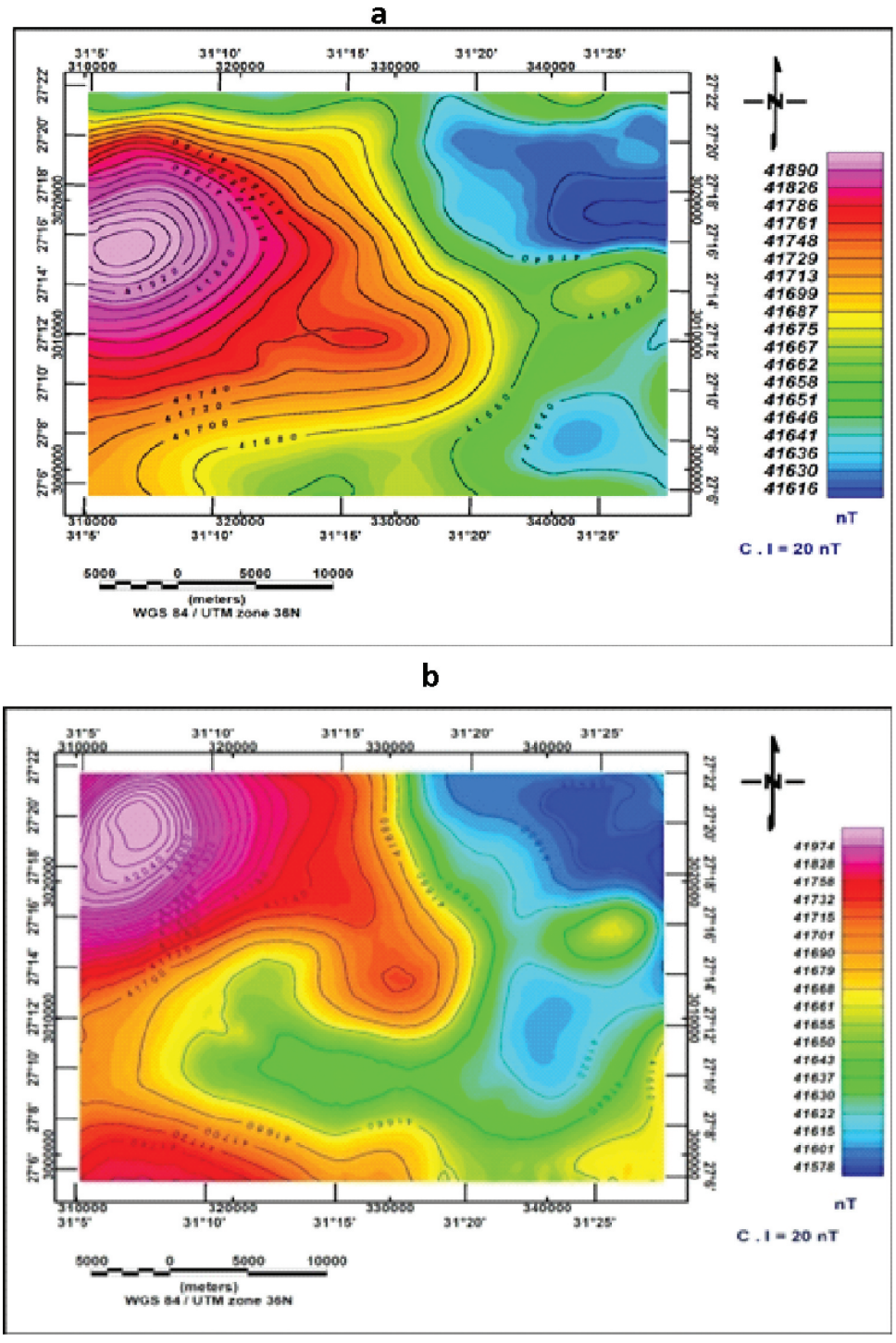

Figure 2. The total magnetic intensity map, b: the reduced to magnetic Pole map (RTP).

(Figure 2(b)) shows a northwestward shift in the locations of the inherited magnetic anomalies as a result of the removal of the magnetic field's inclination at this location. The RTP map displays a variety of magnetic anomalies between 41,578 and 41,974 nT. While the northeastern portion of the region has mild magnetic anomalies, the northwestern and southwestern portions show strong magnetic anomalies.

3.2. Geoelectrical data

3.2.1. Geoelectrical data acquisitions

The geoelectrical data is adjusted using the twenty-nine Vertical Electrical Soundings (VES) of AB/2 on the Schlumberger array, which range from 1.5 to 500 m. (Figure 3(a)), in areas where six geoelectric cross-sections could be built. Each cross-section includes several VESs in addition to the existing water wells.

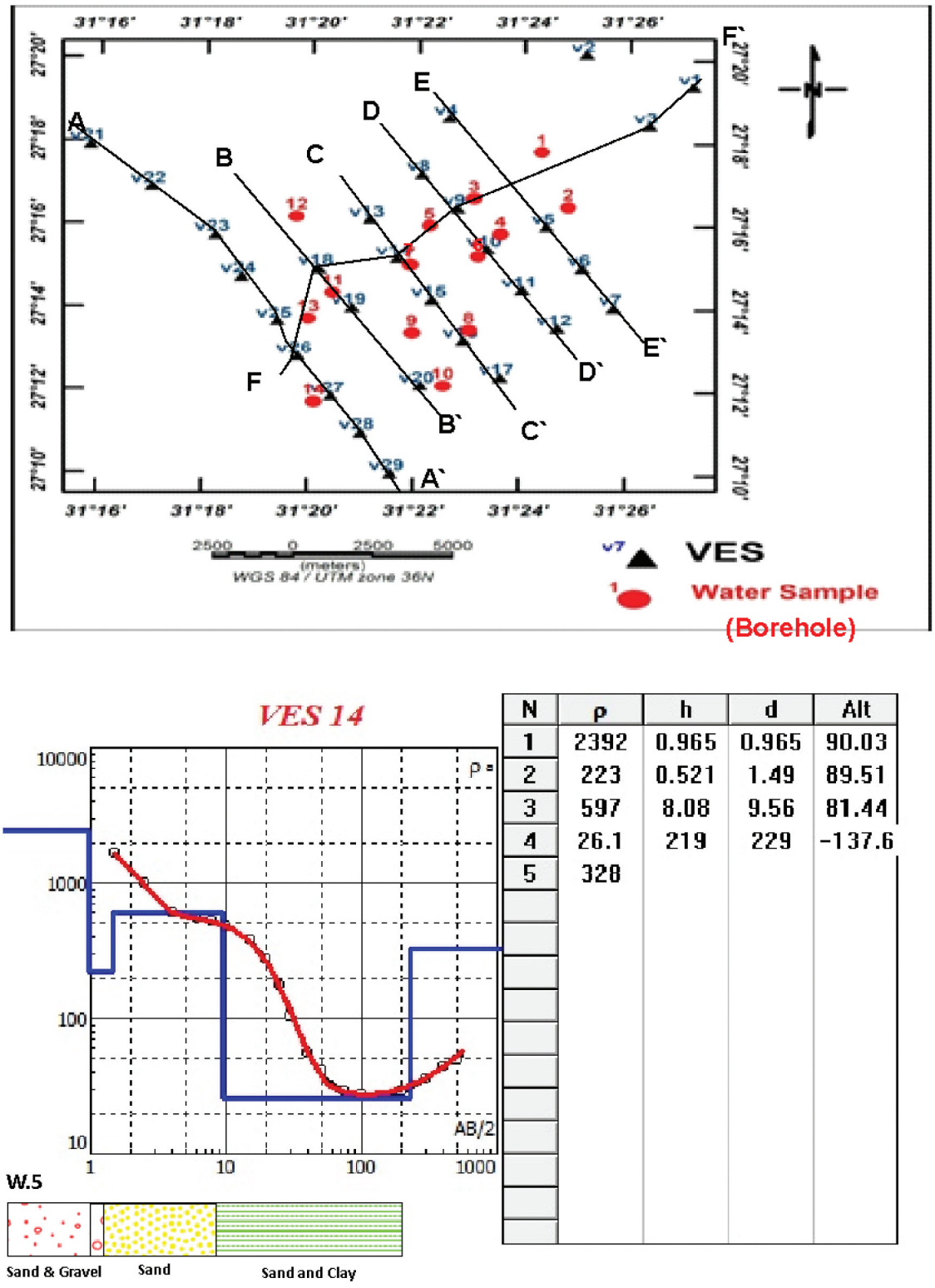

Figure 3. Location map of the VES stations, b: comparison between Well(4) and VES No. 14.

4. Results and discussion

4.1. Results of magnetic data

4.1.1. Euler deconvolution

The main use of the Euler deconvolution potential field interpretation technique is finding the depths of magnetic and gravitational anomalies. Euler's homogeneity equation serves as the foundation for the Euler deconvolution method. The location of the potential source for the degree of homogeneity N can be viewed as a structural index (Thompson 1982). Euler's deconvolution is a common name for this inversion technique. A RTP map was subjected to the Euler approach for various structure indexes (SI), with SI = 0, 1, and 2 corresponding to contact/step, sill/dyke, and cylinder/pipe, respectively (Oasis Montaj 2015). The research area was subjected to the Euler deconvolution approach with SI = 0 (Figure 4(a)), which produced a variety of solutions that pointed to numerous structures, including contact, and step structures. For the interpreted structural lineaments, rose diagrams (Figure 4(c)) were made to help identify the main structural tendencies in the future of the research topic (Figure 4(b)). The results show that the principal trends of the research region are N-S, NNE-SSW, N E-SW, and NW-SE (Figure 4(c)).

4.1.2. 2-D magnetic modeling

The 2-D magnetic modelling is applied on nine profiles, four of them in the south-north direction of the length of 31 km, and the other five profiles in the direction west-east of the length of 37 km for RTP data. The 2-D magnetic modelling is applied using a geosoft package (Oasis Montaj 2015), using the average magnetic susceptibility of 0.000750 CGS units (Araffa et al. 2015). The results of 2-D magnetic modelling refer to the depth of basement rocks ranging from 1680 to 4950 m. Consequently, the thickness of the sedimentary deposits decreases in the northwest (Figure 5).

4.2. Results of geoelectrical data (VES)

The target of interpretation of geoelectrical data is the determining true resistivity and thickness of each geoelectric unit, to achieve this goal two techniques of quantitative interpretation of VES data are used, the first one is a manual interpretation process that relies on generalised Cagniard graphs and two layers of master curves to match the shown field curves (Koefoed 1960; Orellana and Mooney 1966). The second technique is the analytical technique which uses the model manual technique as an initial model through the IPI2WIN software (Bobachev et al. 2008). The results of interpretation for geoelectrical data indicate that the subsurface consists of three strata, with resistivity values ranging from 3.5 to 39,000 Ohm m (due to the gravel and sand boulders) and thicknesses varying from 2 to 150 m, according to

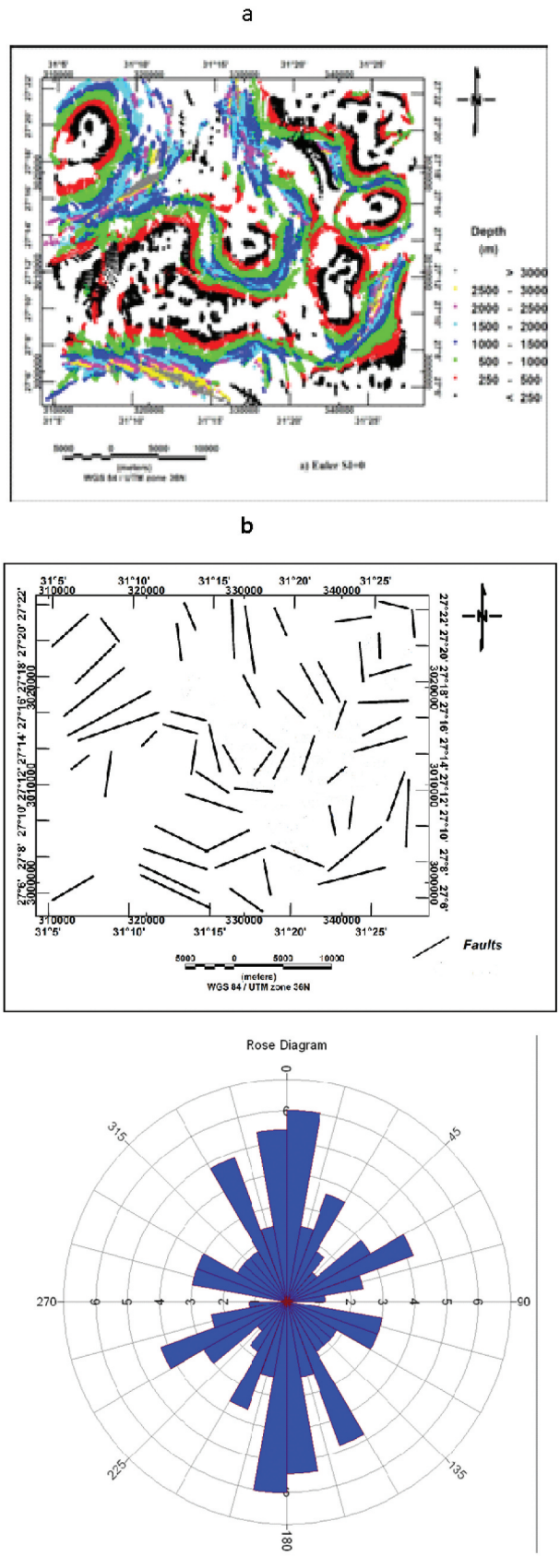

Figure 4. Euler solution with SI = 0, b: structural lineaments as interpreted from Euler with SI = 0, c: Major trend faults dissecting from Euler with SI = 0.

the findings of the analysis of the VESes data. VES No. 14 and Borehole No. 5 were measured side by side for correlation (Figure 3(b)). The lateral and vertical

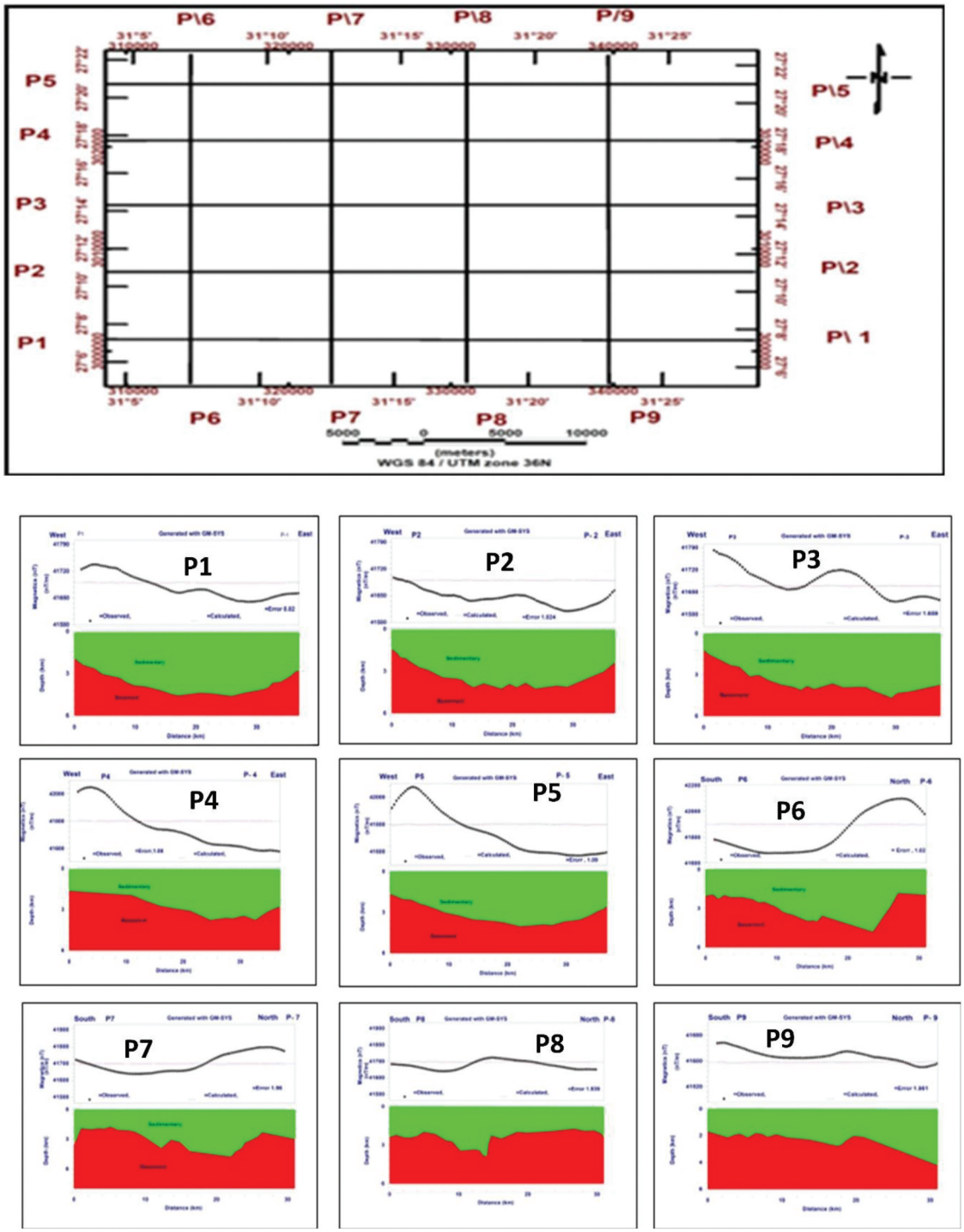

Figure 5. Location of magnetic profiles in the study area, b: 2-D magnetic modelling along profiles P1-P9.

distribution of the subsurface resistivity is shown in the geoelectric cross-sections (Ismail 2003). Six thorough geoelectric cross-sections were built utilising the findings from the modelling of VES stations, which were calibrated using all drilled borehole data and geological information (Figure 3(a)). Figure 6 represents the geoelectric cross-sections along profiles A, B, C, D, E, and F were built to look into the lithological distribution succession. The geological–geoelectrical study reveals that the subsurface is made up of three distinct geoelectrical units. The first unit is a surface layer that exhibits extremely high resistivity values, which correspond to dry sand and gravel boulders. These values range from 465 Ohm.m to 39,000 Ohm.m, with a thickness range of 2–17 m. A second unit is a middle unit with low resistivity values ranging from 3.5 to 37 Ohm.m and variable thicknesses between 151 and 260 m. Sand, clayey sand, and intercalated sandy clay make up this unit. All drilling data show that the second unit is saturated with groundwater, and this unit contains groundwater of various salinities. The third geoelectric unit exhibits high resistivity values matching Eocene limestone, ranging from 123 Ohm.m to 776 Ohm.m.

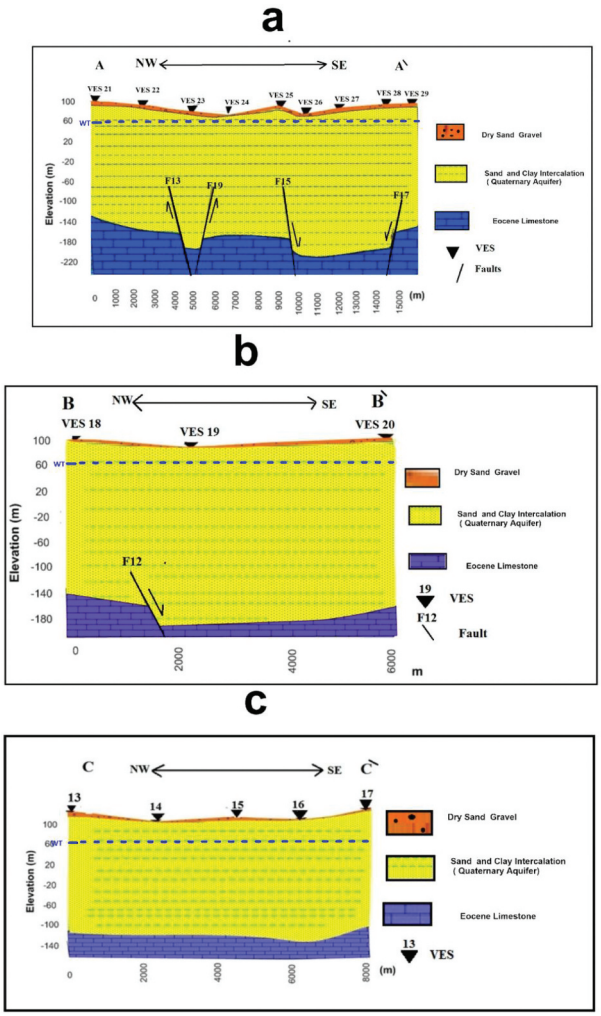

Figure 6a. Geoelectric cross-sections along profiles A-A`, B-B` and C-C`.

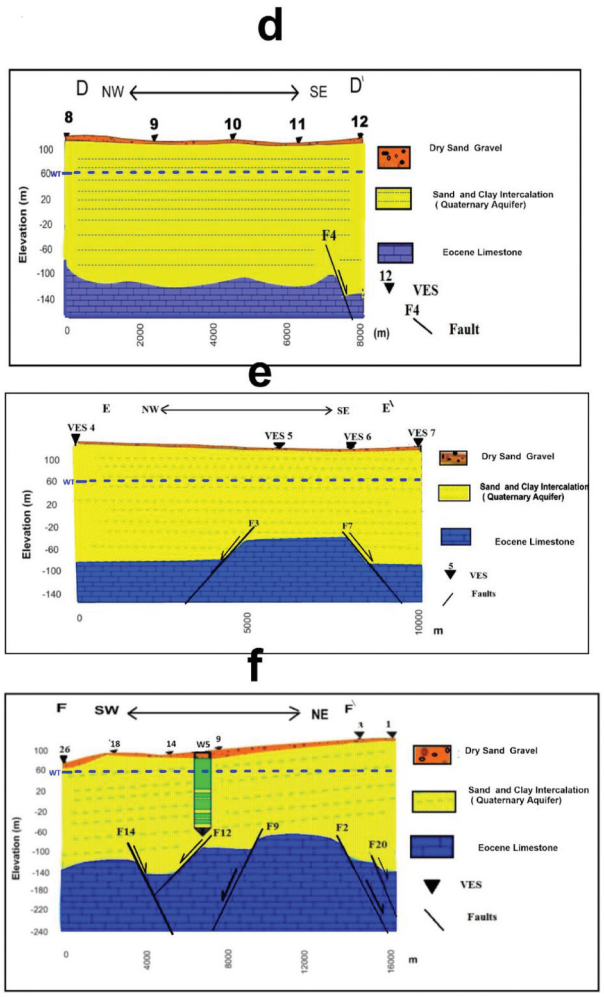

Figure 6b. Geoelectric cross-sections along profiles D-D`, E-E` and F-F`.

4.2.1. Isoresistivity and isopach maps of the aquifer

The isoresistivity map for the second geoelectric unit, which represents the aquifer in the studied area, reveals an increase in resistivity at VES no.18 and 19 in the northwest due to an increase in sand content and a decrease in resistivity in the middle and northeast due to an increase in clay content (Figure 7(a)). According to the water-bearing layer's isopach map, the thickness of the aquifer grows downstream of Wadi El-Assiuty and diminishes upstream in an easterly direction (Figure 7(b)).

5. Hydrogeological and hydrochemistry data

The Quaternary aquifer, which has a thickness of roughly 200 metres and is quite productive, is made up of graded sand and gravel with thin interbeds of clay. It takes up a large portion of the Nile Valley and is protected by an aquitard of Holocene silty clay. Various writers, including Wade et al. (2012), examined the hydrochemistry of groundwater (2013). This aquifer has somewhat restricted groundwater (Said 1990). The objective of the current study's hydrochemical examination is to identify the physical characteristics and relative abundances of groundwater's main ions. The place of the investigated wells is depicted in (Figure 3(a)). Fourteen wells were drilled to different depths varying from 140 to 202 m. The groundwater samples were analysed for physical properties such as specific electric conductivity (EC), pH measurements, and chemical properties, including the concentrations of major ions (potassium, sodium, magnesium, calcium, chloride, sulphate, and bicarbonate). The chemical analyses were carried out in the General Company for Research and Groundwater (RGWA) laboratories in 2017 according to the standard methods. The water table data from drilled borehole are used to construct water table map (Figure 8(a)). The water table map refers to the water level at elevation ranged from 50 to 60 m, the water flow direction is from southwest to northeast direction.

5.1 Physical parameters of groundwater

5.1.1. The pH measurement

Using a laboratory pH metre, Model WTW-Multilane pH Germany, with an accuracy of 1%, which gives direct results of the pH values, the pH values of the various tested substances were assessed. Pure water has a pH of 7

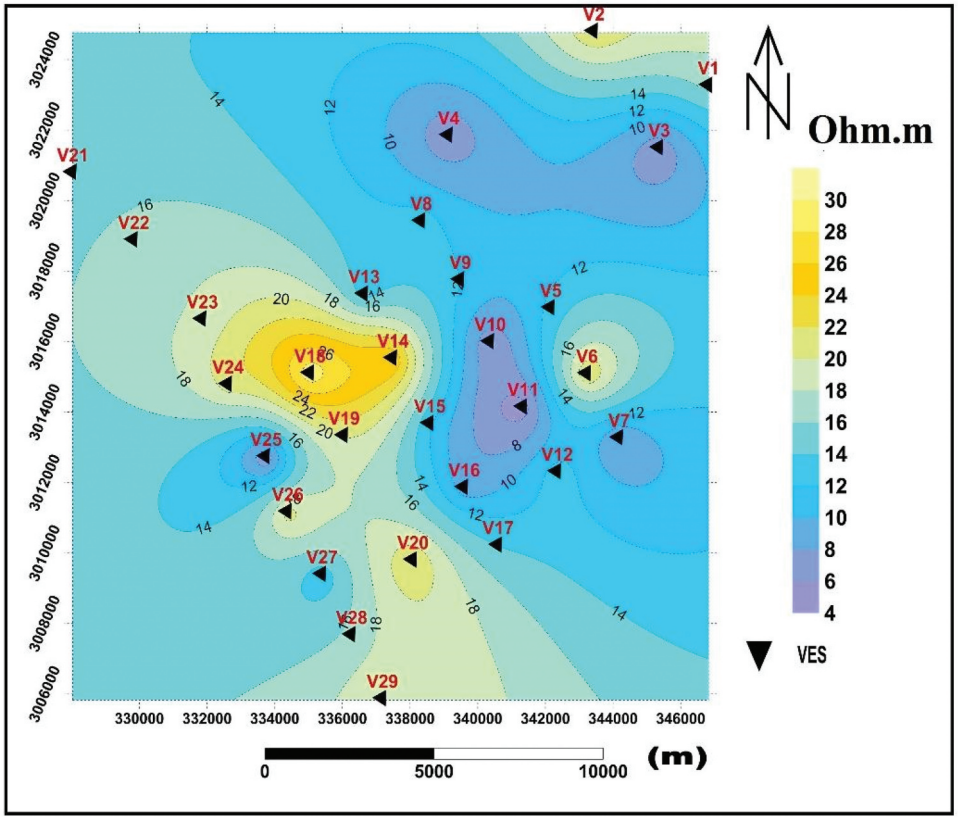

Figure 7a. (Continued).

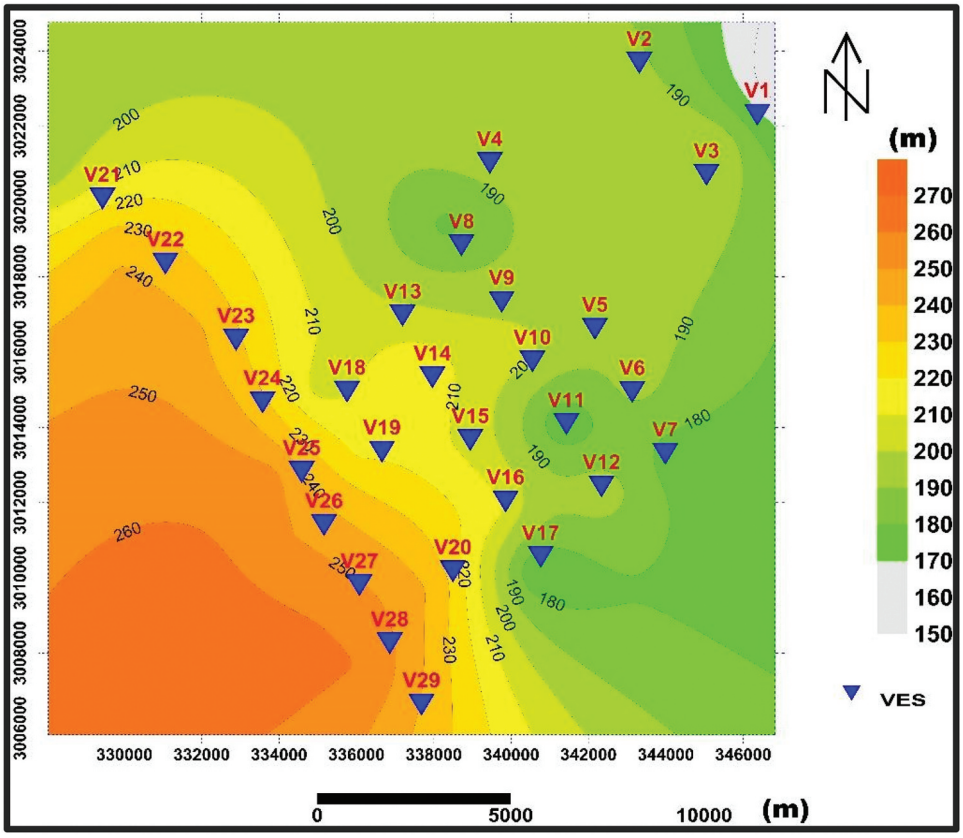

Figure 7b. True resistivity map for second geoelectric unit (water-bearing layer), b: isopach map for water-bearing layer.

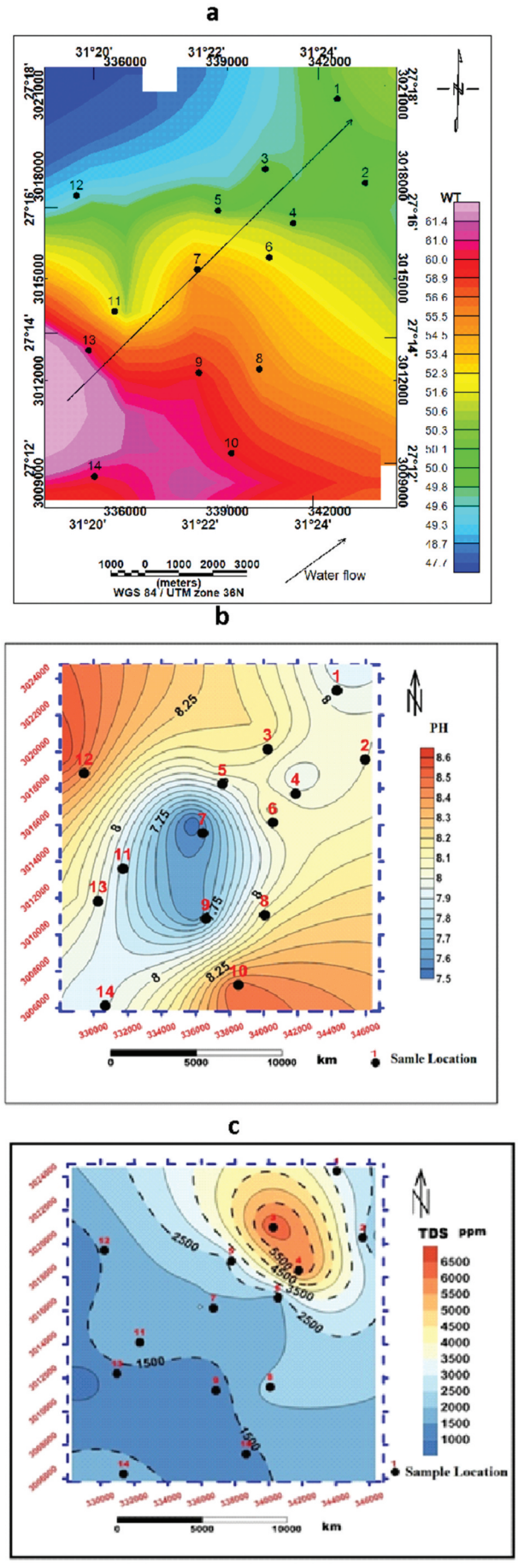

Figure 8. Physical parameters of groundwater, a: water table map, b: PH values, c: total dissolved salts (TDS).

at 25 degree Celsius, but when exposed to atmospheric carbon dioxide, this equilibrium results in a pH of roughly 5.2 (Forstner and Wittman 1983). It is based on how temperature and air gases interact with pH. The pH ranges from 7.5 to 8.6 (Figure 8(b)). The groundwater in the research region is mild to moderately alkaline, as evidenced by the minimum value of 7.5 discovered in well No. 7 in the centre of the area and the maximum value of 8.60 found in wells No. 12 in the northwestern part and No. 10 in the southern half.

5.1.2. Total dissolved salts (TDS)

The average salinity of the groundwater in the study area is 3646.5 mg/l, with salinities ranging from 819 mg/l to 6474 mg/l. At well No. 13, which is situated towards the region's downstream, in the western portion of the research area, the minimum salinity of 819 mg/l was observed. The groundwater salinity (TDS) (Figure 8(c)) shows how the relatively low salinity along the NW fault zone restricts water flow and is suggestive of the rapid rate of recharge from the Nubian Sandstone aquifer's deep-seated dynamic fault. Due to the relatively low rates of recharge from the eastern watershed area, which is renowned for its marine-nature rocks, the salinity rises as one moves east (limestone and marl). The research area's groundwater has an average salinity of 3646.5 mg/l and a salinity range of 819 mg/l to 6474 mg/l. In well No. 13 to the west of the analysed area, which is situated downstream of the research area, the minimum salinity of 819 mg/l is observed. The groundwater salinity map (Figure 8c) demonstrates that the rapid rate of recharging from the Nubian Sandstone aquifer through a deep-seated dynamic fault is the cause of the relatively low salinity along the NW-SE fault plain. The salinity increases eastward due to the relatively slow rate of recharge from the eastern watershed area, which is known for its marine-nature rocks (limestone, marl).

5.2. Distribution of Major elements

5.2.1. Major cations

5.2.1.1. Potassium (K^+). Humans require potassium, which is rarely or never present in drinking water in quantities that would be dangerous for healthy people. Despite not being water soluble, potassium reacts with water in the following ways: $2K + 2\,h_2O = 2KOH + h_2$, where (g) Potassium and water react quickly and vigorously to produce hydrogen gas and a colourless basic potassium hydroxide solution. The groundwater in the study area has a potassium level that ranges from 3 to 144.1 mg/l on average. The investigated area's well number 3 on its northern side recorded the highest value, while well number 7 in its centre recorded the least amount of substance (Figure 9a).

5.2.1.2. Sodium (Na^+). The majority of sodium salts are extremely soluble in water and leach into groundwater and surface waters from the terrestrial environment. We may infer from the chemical analysis results that the content of sodium in groundwater is significantly higher in the eastern ward direction than the recommended value. The sodium concentration ranges from 126 to 1950 mg/l (Figure 9b), with an average of 1038 mg/l. Well number 13 is located on the western side of the research area with lowest salinity, while well number 4 is positioned on the northeastern side, with the highest value being recorded there. While the groundwater of the northeastern side of the studied area is distinguished by a relatively high content of sodium ions (Na+), which varied between 500 and 1950 mg/l with an average of 1225 mg/l, the concentration is less than 500 mg/l.

5.2.1.3. Magnesium (Mg^{+2}). The magnesium level in the current study ranges from 24 to 220 mg/l, with an average of 122 mg/l (Figure 9c). The tested area's well number 12 had the lowest concentration (24 mg/l), whereas well number 3 on the northeastern side had the highest (220 mg/l). Due to the pollution of groundwater by a modest rate of recharge from the eastern watershed area, which is distinguished by rocks of a marine origin, the magnesium content rises towards the east from 80 to 220 mg/l.

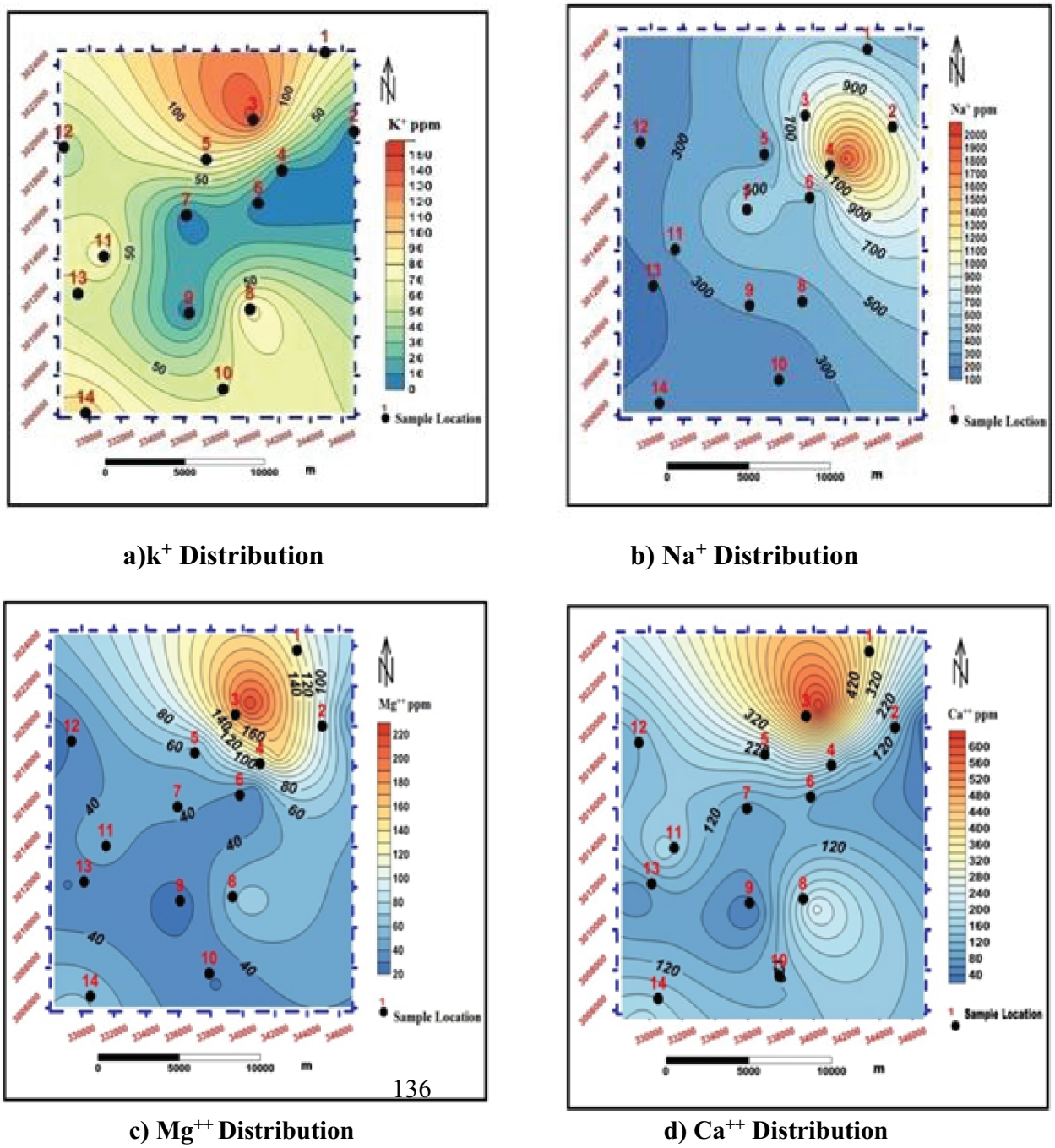

a)k^+ Distribution

b) Na^+ Distribution

c) Mg^{++} Distribution

d) Ca^{++} Distribution

Figure 9. Assembled cations contour maps.

5.2.2.4. Calcium (Ca^{+2}). The calcium ion concentration in the current study ranges from 23.97 to 625 mg/l, with an average of 324.5 mg/l; well number 13 on the western edge of the analysed area had the lowest value (23.97 mg/l). While there is a general increase in calcium concentration eastward, the highest value (625 mg/l) was discovered in well number 3 on the northeastern side of the analysed area (Figure 9d).

5.2.2. Major Anions

5.2.2.1. Chloride (Cl^{-}). Chloride is the most prevalent major anion in natural water since it is only found in nature in combination with other elements, primarily sodium in the form of common salt (NaCl). The average chloride concentration in the study region is 1687.5 mg/l, with a range of 175 mg/l to 3200 mg/l. The well with the lowest value, number 13, was found on the western side of the study area, and the well with the highest content, number 4, was found on the northeastern side of the study area (Figure 10a).

5.2.2.2. Sulfate ($SO_4)^{-2}$. Sulphate is a naturally occurring substance that can be found in various minerals, such as gypsum and barite ($BaSO_4$) ($CaSO_4$). Sulphate ions may drain from top surface soil sediments in such arid areas, raising the concentration of these ions in groundwater. Gypsum and anhydrite are the most common sulphate sources in

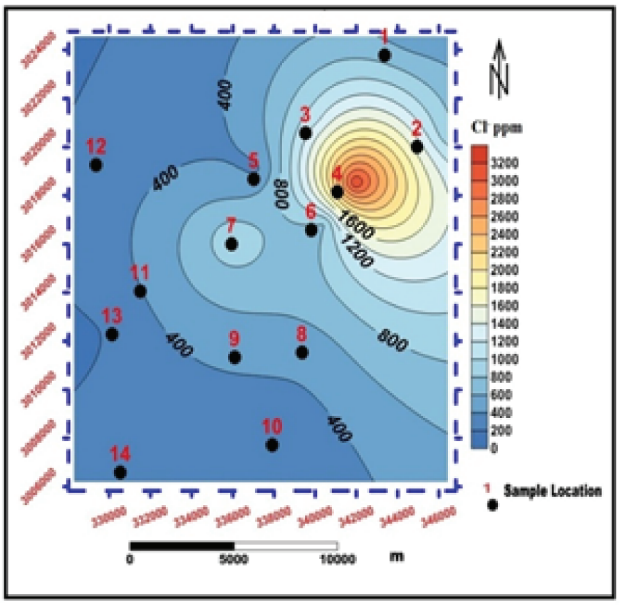

a) Cl Distribution

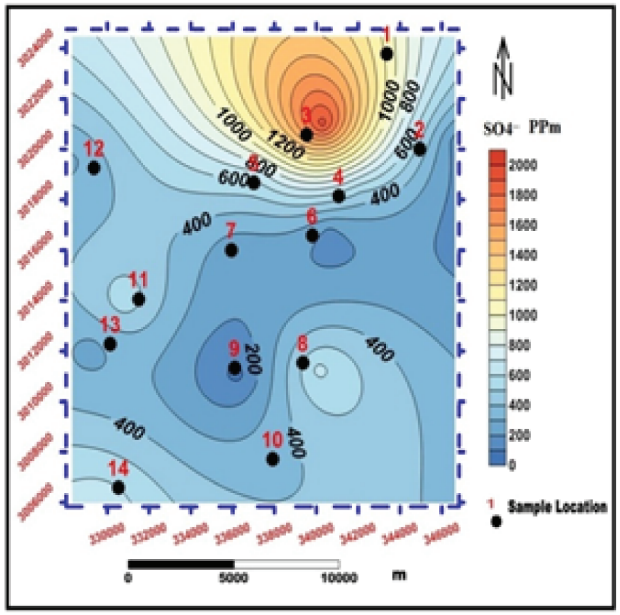

b) SO_4 Distribution

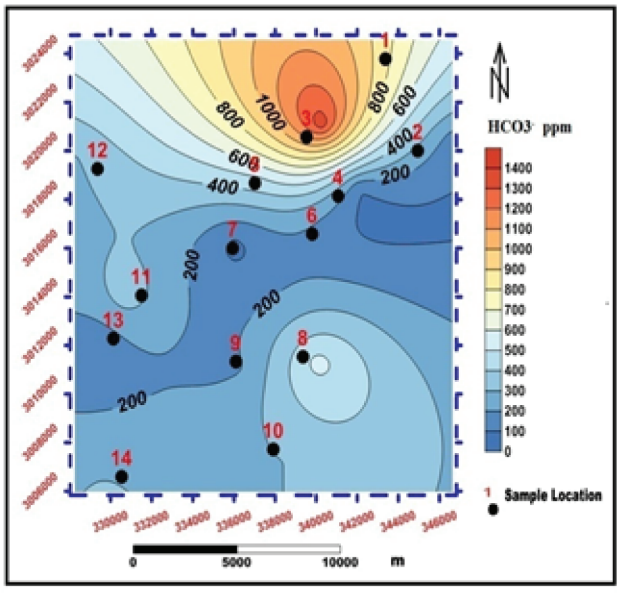

C) HCO_3 Distribution

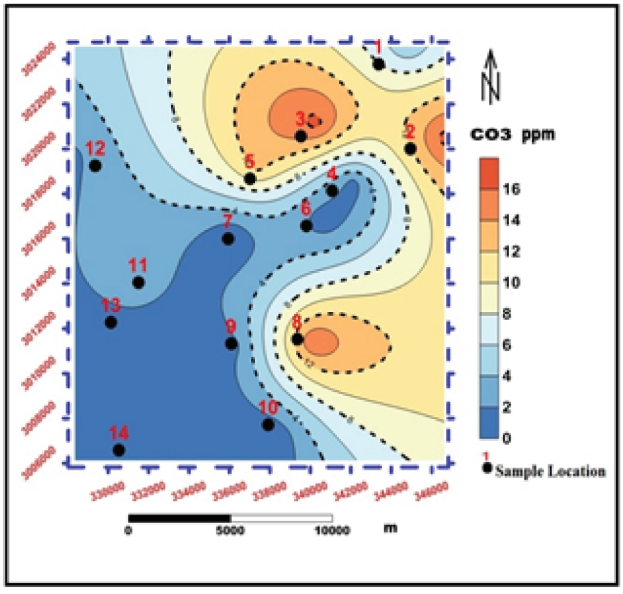

d) CO_3 Distribution

Figure 10. Assembled anions contour maps.

groundwater. At normal temperatures, gypsum easily disintegrates in water. With a range of 70.3 to 1954 mg/l, the research area's average sulphate content is 1012.15 mg/l (Figure 10b). The centre of the region's well No. 9 showed the lowest value (70.3 mg/l). The highest concentration (1954 mg/l) was found in well number 3 in the northeastern portion of the study region.

5.2.2.3. Carbonates (CO_3) and bicarbonates $(HCO_3)^-$. The carbonates and bicarbonates (HCO_3) in the water are what cause the hardness and alkalinity. The pH level is influenced by the relative concentrations of carbonates, bicarbonates, and carbonic acid in water. Calcite ($CaCO_3$) is the primary form of carbonates found in soil. In the study region, bicarbonate concentrations ranged from 76 to 1360 mg/l, with an average of 718 mg/l. Well, No. 7 in the centre of Wadi El Assiuty recorded the lowest value (76 mg/l), and Well No. 3, which is located to the north of the study region, recorded the highest value (1360 mg/l) (Figure 10c).

5.3. Water type

Piper's classification (Piper 1953) is widely recognised as a valuable tool for interpreting water analysis, aiding in the classification of water and the identification of hydrochemical facies within mixed water samples. This classification method relies on the proportional equivalence of cations and anions, focusing on their relative ratios rather than their absolute amounts. The resulting Piper diagram illustrates these relative ratios by projecting information from two triangles onto a diamond-shaped plot. One line is drawn through the point on the cation triangle, while another is drawn through the anion triangle. The intersection of these lines determines the point's location on the Piper diagram's diamond-shaped portion, enabling the identification of water types. Additionally, the Piper diagram facilitates the categorisation of waters into hydrogeochemical facies. For instance, if a water plot appears near the centre of one of the triangles' edges, it may indicate a non-standard water type, such as magnesium-calcium sulphate water. Using this classification method, groundwater in wells 1, 3, 5, 10, 11, 13, and 14 are classified as Sodium Sulphate water type, while groundwater in wells 2, 4, 6, 7, 8, 9, and 12 are classified as Sodium Chloride water type, according to the Piper diagram. The significance of Piper's classification approach is emphasised, along with how it may be used to identify different types of water and how to apply Piper's Diamond plot standard classification (Piper 1953), (Figure 11).

5.4. Priority map for future drilling

The priority map (Figure 12) refers to the western part of the area that is suitable for future drilling which is represented as zone A. where the western part has a low salinity of high-quality water for drinking, agricultural, and industrial purposes.

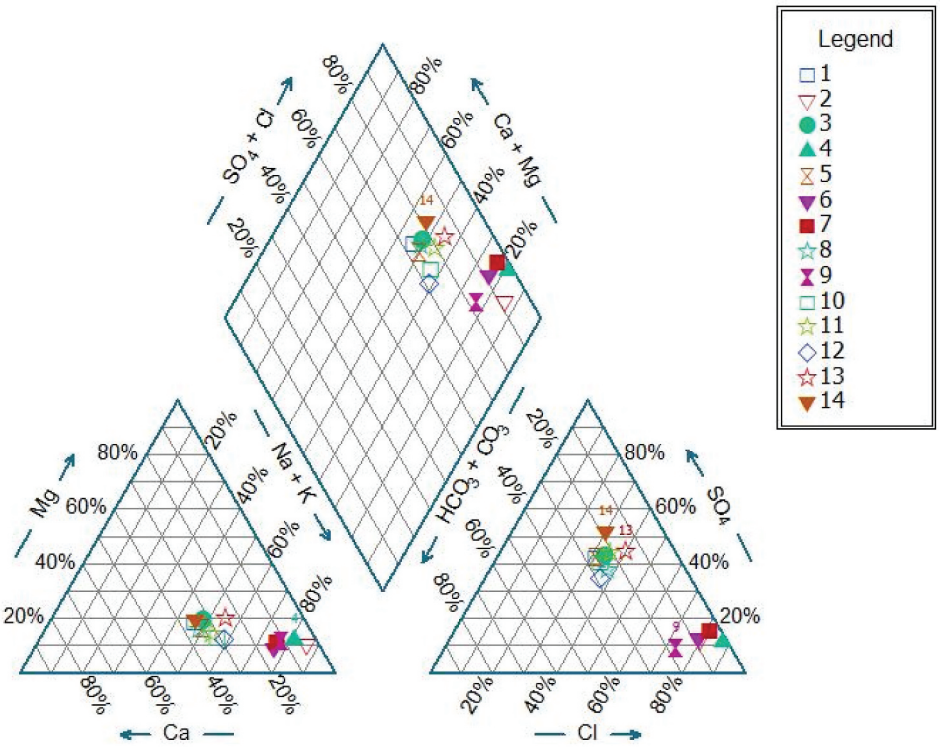

Figure 11. Determination of hydrogeochemical facies using piper diagram.

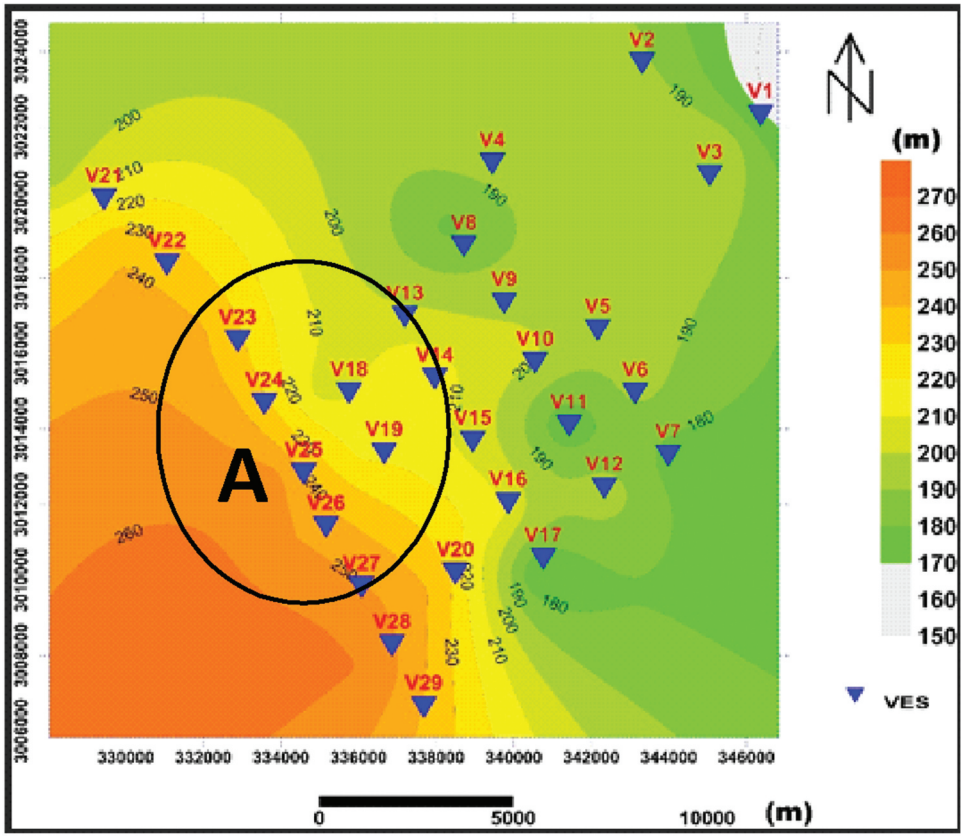

Figure 12. Priority map for future drilling.

6. Discussion

The area under investigation is situated in the westernmost portion of the Eastern Desert. Therefore, the authors used a variety of geophysical techniques to identify the structural components that cut through the sedimentary layer and they suggested locations for future boreholes. The magnetic approach was employed to measure the thickness of the sedimentary layer in the research region in order to first determine the depth of the basement complex. The geologic map shows that the research area is divided by several faults that are part of the major NE-SW and NW-SE trends. These trends also have subsurface extensions, which are referenced in the analysis of magnetic data. The information from boreholes shows that the study area is covered by a groundwater aquifer with a range of salinities. Additionally, the interpretation of geoelectrical data is in line with the parameters of the groundwater aquifer, including its thickness, water level, and water quality, through the values of resistivity. Geoelectrical data interpretation shows that the subsurface is composed of three layers, including sand and gravel, sandy clay, and limestone. This order is by the geologic environment of the research region. The interpretation of VES No. 14's results demonstrates strong agreement with the drill data for Business Well (4). The results of the data from the boreholes show that the resistivity values for the water-bearing zone are consistent with the total amount of dissolved salts (aquifer). The western part of the study area is the best site for future drilling which is characterised by the high thickness of the aquifer and high resistivity (more fresh water less salinity) as shown in Figure 7c

7. Conclusion

These are some of the inferences that can be taken from an interpretation of the geophysical data: Between 1800 and over 4500 m is the depth at which the basement rock can be found. The investigation is focused mostly in the east-west, north-northeast-southwest, northeast-southwest, and northwest-southeast directions. In the area that is the subject of this research, the stratum containing water is an aquifer made up of sandy clay, sand, and clayey sand. The drilling of water wells revealed that this area is rich in a variety of groundwater sources to a very high concentration. The geoelectric data interpretation indicates that the aquifer's depth ranges from 6 to 18.4 m, and thickness ranges from 150 to 250 m with resistivity values of 4–30 Ohm.m. In the area under study, the potassium content of the groundwater ranges from a minimum of 3 mg/l to a maximum of 144.1 mg/l on average. The sodium concentration ranges anywhere from 126 to 1950 mg/l throughout the mixture. The magnesium concentration rose from 24 to 220 mg/l throughout the experiment. The chloride concentration in the area that was

investigated varied from 175 mg/l to 3200 mg/l, with 1687.5 mg/l serving as the mean value. Sulphate concentrations in the region under study range from 70.3 to 1954 mg/l, with a mean value of 1012.15 mg/l and a standard deviation of 102.15 mg/l. The Piper diagram indicates that the groundwater in wells 1, 3, 5, 10, 11, 13, and 14 are classified as Sodium Sulfate water type, while groundwater in wells 2, 4, 6, 7, 8, 9, and 12 are classified as Sodium Chloride water type. In a broad sense, the thickness of the aquifer grows thinner moving upstream in an easterly direction towards Wadi El-Assuity, and increases as one moves downstream. The best site for future drilling is the western part of the study area.

Disclosure statement

No potential conflict of interest was reported by the author(s).

Funding

The author(s) reported that there is no funding associated with the work featured in this article.

Authors' contributions

All authors have contributed to writing the manuscript, interpretation of data, and drawing the figures.

Availability of data and material

The datasets used and/or analysed during the current study are available from the corresponding author upon reasonable request.

References

Abdo AM, Sabet HS, Mebed ME. 2021. Lineaments detection and groundwater exploration using gis and geo-electric data at Wadi El-Asyuti Area, Eastern Desert, Egypt. Al-Azhar Bull Sci Sect D. 32(2):49–59. doi: 10.21608/absb.2021.84781.1125.

Aero-Service. 1985. Interpretation report: airborne gamma-ray spectrometer and magnetometer survey of the Eastern Desert of Egypt, area-ii. Aero service division, western geophysical Co of america. Houston (TX), USA, 127.

Araffa SAS, El Nabi SH, Helaly AS, Dawoud MA, Sharkawy MS, Hassan NM. 2022. Groundwater aquifer assessment using hydrogeophysical investigations: the case of western Al Ain Sokhna area, Gulf of Suez, eastern desert. Egypt Geocarto Int. 37(27):16512–16533. doi: 10.1080/10106049.2022.2109762.

Araffa SAS, Sabet HS, Gaweish WR. 2015. Integrated geophysical interpretation for delineating the structural elements and groundwater aquifers at central part of Sinai peninsula. Egypt J Afr Earth Sci. 105:93–106. doi: 10.1016/j.jafrearsci.2015.02.011.

Azmy EM, El-Wer A, Helaly AS, Araffa SAS, Farag KSI. 2023. Joint electromagnetic-terrain conductivity and DC-Resistivity survey for bedrock and groundwater characterization at the New Al-Obour City, Egypt. Iraqi Geological J. 56(1C):262–276. doi: 10.46717/igj.56.1C.18ms-2023-3-29.

Bobachev A, Modin I, Shevnin V. 2008). IPI2WIN v.3.1, User's Manual Bresler, E. McNeal, B. I. and Carter, D. L. 1982: Saline and Sodic Soils PrincipalsDynamics-Modeling, Spring-Verlag, Berlin, ISBN: 978-3-642-68326-8 (Print) 978-3-642-68324-4 (Online), 236 P.

Deep AL, Araffa M, Mansour SAS, Mansour SA, Taha AI, Mohamed A, Othman A. 2021. Geophysics and remote sensing applications for groundwater exploration in the fractured basement: a case study from Abha area. Saudi Arabia, J Afr Earth SciencesVolume. 184:104368. doi: 10.1016/j.jafrearsci.2021.104368.

Elbarbary S, Araffa SAS, El-Shahat A, Abdel Zaher M, Khedher KM. 2021. Delineation of water potentiality areas at Wadi El-Arish, Sinai, Egypt, using hydrological and geophysical techniques. J Afr Earth SciencesVolume. 174:Article number 104056. doi: 10.1016/j.jafrearsci.2020.104056.

El Miligy EM. 2003. Groundwater resources evaluation of Assuit Governorate [Ph. D. thesis;]. Fac. Sci. Assuit Univ. Egypt, 190.

El Shemi AM, Setto I, Mauritsh HI, Abu Helkia MM. 1999. The delineation of surface and subsurface structures in the area between El minia and Assiut, Egypt, Bull. Fac Sci Assiut Unv. 28(2–f):161–190.

Farrag AA, Ebraheem MO, Sawires R, Ibrahim HA, Khalil AL. 2018. Petrophysical and aquifer parameters estimation using geophysical well logging and hydrogeological data, Wadi El-Assiuoti, eastern desert. Egypt J Afr Earth Sci. 149:42–54. doi: 10.1016/j.jafrearsci.2018.07.023.

Forstner U, Wittman GTW. 1983. Metal pollution in the aquatic environment. 2nd ed. pp. 481. (NY): PLO, Spring-Veriag.

Ismail AM. 2003. Geophysical, hydrological and archaeological investigation in the East Bank of Luxor, Ph [D. thesis]. Department of Geology and Geophysics, University of Missouri-Rolla, 211.

Koefoed O. 1960. Geosounding principles resistivity sounding measurements, elsevier. Amsterdam: Science Publishing. Company.

Mansour HH, Philobbos IR. 1983. Lithostratigraphic classification of the surface Eocene carbonate of the Nile Valley, Egypt. Bull Fac Sci Assiut Univ. 2(2):129. 153.

Mohamed A, El Ella A, El M. 2021. Magnetic applications to subsurface and groundwater investigations: a case study from Wadi El Assiuti, Egypt. Int J Geosciences. 12(2):77–101. https://www.scirp.org/journal/ijg.

Mohamed AME, Araffa SAS, Mahmoud NI. 2012. Delineation of near-surface structure in the southern part of 15th of May City, Cairo, Egypt using geological, geophysical and geotechnical techniques. Pure Appl Geophys. 169(9):1641–1654. doi: 10.1007/s00024-011-0415-y.

Mohamed K. 2013. Investigation of the subsurface geologic section and groundwater potentiality in Wadi Al-Assuity Area, Eastern Desert, Egypt, using seismic refraction method. Geological Soc Am Abstr Programs. 45(7):162.

Nazih M, Gobashy M, Araffa SAS, Soliman KS, Abdelhalim A. 2022. Geophysical studies to delineate groundwater aquifer in arid regions: a case study, Gara Oasis, Egypt. Contrib Geophys Geod. 52(4):517–564. doi: 10.31577/congeo.2022.52.4.2.

Oasis Montaj 8.4. 2015. Geosoft provides data processing and analysis (DPA) software and services for geological,

geophysical, geochemical, UXO detection, and environmental applications prospecting and remote sensing. Cambridge University Press.

Orellana E, Mooney HM. 1966. Master table and curves for vertical electrical sounding data. Geophys Prospect. 8 (3):459–469.

Piper AM. 1953. A graphic procedure in the chemical interpretation of water analysis. US Geological Survey Groundwater Note. 12.

Ramadan TM, Sultan SA. 2004. Integration of remote sensing, geological and geophysical data for the identification of massive sulphide zones at Wadi Allaqi area, South Eastern Desert, Egypt M.E.R.C. Ain shams univ. Earth Sci Ser. 18(2004):165–174.

Said R. 1990. The geology Egypt. In Balkeme AA, editor. RoHerdam – Broof Field; p. 734.

Sultan SA, Santos FAM. 2008. Evaluating subsurface structures and stratigraphic units using 2D electrical and magnetic data at the area north Greater Cairo, Egypt. Int J Appl Earth Observation And GeoinformationVolume. 10 (1):56–67. doi: 10.1016/j.jag.2007.05.001.

Thompson DT. 1982. EULDPH, a new technique for marking computer-assisted depth estimates from magnetic data. Geophysics. 47(1):31–37. doi: 10.1190/1.1441278.

Wade AJ, Palmer-Felgate EJ, Halliday SJ, Skeffington RA, Loewenthal M, Jarvie HP, Bowes MJ, Greenway GM, Haswell SJ, Bell IM, et al. 2012. Hydrochemical processes in lowland rivers: insights from in situ, highresolution monitoring, Hydrol. Hydrol Earth Syst Sci. 16(11):4323–4342. doi: 10.5194/hess-16-4323-2012.

Yan E, Wagdy A, Sultan M, Becker R. 2004. Assessment of renewable groundwater resources in the assuity hydrologic system of the eastern desert, Egypt. Second Regional Conference on Arab Water, Action Plans for Integrated Development. p. 11.

Yousef AF. 2008. The impact of north west active fault system on the recharge of the quaternary aquifer system around the Nile Valley: case study Wadi El Assiuti, Eastern Desert, Egypt. Eur Water. 21(22):41–55.

Youssef MI. 1968. Structural pattern of Egypt and its interpretation. The amer. Assoc Petroleum Geologist Bulktin. 52(4):601–614. doi: 10.1306/5D25C44D-16C1-11D7-8645000102C1865D.

Youssef MMS, Mansour HH. 1977. Subsurface structural study of the area around Assiut. Egypt, Bull. Fac Sci Assiut Unv PF. 293:306.